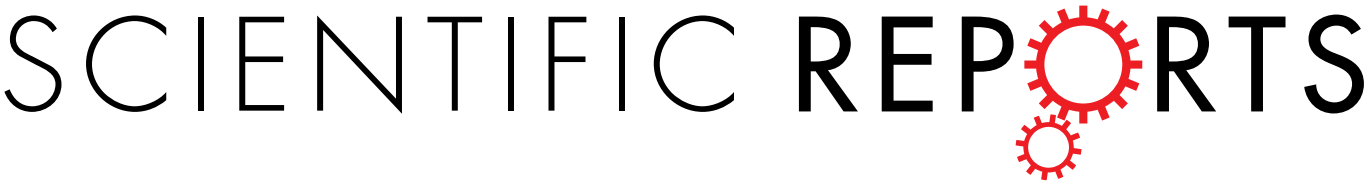

OPEN

Plasmon-Enhanced Photocurrent using Gold Nanoparticles on a Three-Dimensional TiO_2 Nanowire-Web Electrode

Received: 16 September 2016
Accepted: 11 January 2017
Published: 10 February 2017

Yin-Cheng Yen, Jau-An Chen, Sheng Ou, Yi-Shin Chen & Kuan-Jiuh Lin

In this study, an anatase/rutile mixed-phase titanium dioxide (TiO_2) hierarchical network deposited with Au nanoparticles (Au/TiO_2 ARHN) was synthesized using a facile hydrothermal method followed by a simple calcination step. Such a unique structure was designed for improving the light harvest, charge transportation/separation, and the performance of photo-electro-chemical (PEC) cells. The properties of the as-synthesized Au/TiO_2 ARHN in PEC cells were investigated by electrochemical measurements using a three-electrode system in a 1 M NaOH electrolyte. Remarkably, a 4.5-folds enhancement of the photocurrent for Au/TiO_2 ARHN was observed as compared to that for TiO_2 nanowire (NW), under AM1.5G solar illumination, suggesting its potential application in PEC cells. A mechanism has been proposed to explain the high photocurrent of Au/TiO_2 ARHN in PEC water splitting.

Honda and Fujishima elucidated the possibility of water splitting using TiO_2 as electrode[1]. Since then, various TiO_2 nano-architectonic topographies have been greatly desired for enhancing the performance of PEC cells[2–8]. In general, a predominant PEC cell relies on two factors: the efficient usage of solar energy and the instant transportation/separation of charges[9]. Hence, the development of nano-sized photo-active semiconductors to satisfy the requirements has been a long-standing objective in the research of PEC cells, especially for one-dimensional TiO_2 due to its superior charge transport property[10]. To date, many hierarchical TiO_2 nanostructures based on nanowires (NWs) and nanotubes (NTs) have been synthesized for enhanced photo-electric efficiency in solar energy harvesting, conversion, and pollutant purification[11–13]. Such a heterojunction nanostructure would stagger energy levels and scatter incident light to enlarge light absorption in the UV region[14]. However, the strategies for fabricating hierarchical TiO_2 nanostructures have the disadvantages of an extremely time-consuming process, specific/highly expensive fabricating apparatus and back-side illumination, thus making it economically non-competitive[15–25].

Recently, to expand the TiO_2 optical adsorption spectrum from the UV into the visible region, plasmonic electrodes composed of Au/TiO_2 nano-architectonic topographies have been developed with localized surface plasmon resonance (LSPR) property[26–35]. However, most of these reports focus on the discussion of the relationship between particle size/shape/distance/concentration and the photo-electrochemical performance[28–30,32–35]. Especially, one novel example of demonstrating the influence of TiO_2 nanostructure on the LSPR property was reported by Wang *et al.*[36]. An Au/TiO_2/Au nanostructure with a 5-nm-thick TiO_2 middle layer was synthesized which resulted in a maximum 38-fold enhancement of the electric field density of LSPR and about 3-fold improvement of the photocurrent in a wavelength range of 400–650 nm. The enhanced performance is mainly arising from the thickness of TiO_2 satisfying the requirement for generating the coupling effect between the oppositely aligned and nearly touching Au NPs on TiO_2 nanosheet. However, the longer time (4 days) required to synthesize the TiO_2 nanostructures and the non-transparency of the Au/TiO_2/Au film limit their application. Furthermore, there is limited knowledge on how to design and synthesize a TiO_2 nanostructured film on a transparent substrate by a simple yet effective method. Therefore, the aim of this study is to provide a novel strategy for building a new TiO_2 nanostructure to intensify the coupling effect between Au NPs that significantly enhances the photoelectric conversion.

Herein, a three-dimensional (3D) web constructed by Au plasmonic NPs on TiO_2 anatase/rutile hierarchical network (Au/TiO_2 ARHN) is proposed, which is schematically shown in Fig. 1. In order to strengthen the

Department of Chemistry, National Chung Hsing University, Taichung 40227, Taiwan, Republic of China. Correspondence and requests for materials should be addressed to K.-J.L. (email: kjlin@dragon.nchu.edu.tw)

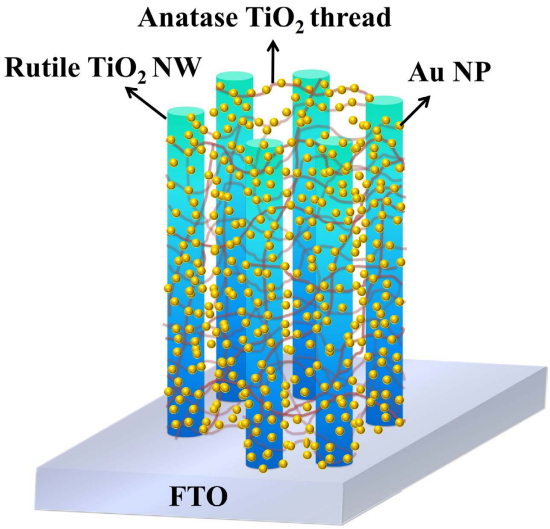

Figure 1. Schematic representation of Au/TiO_2 ARHN on FTO substrates.

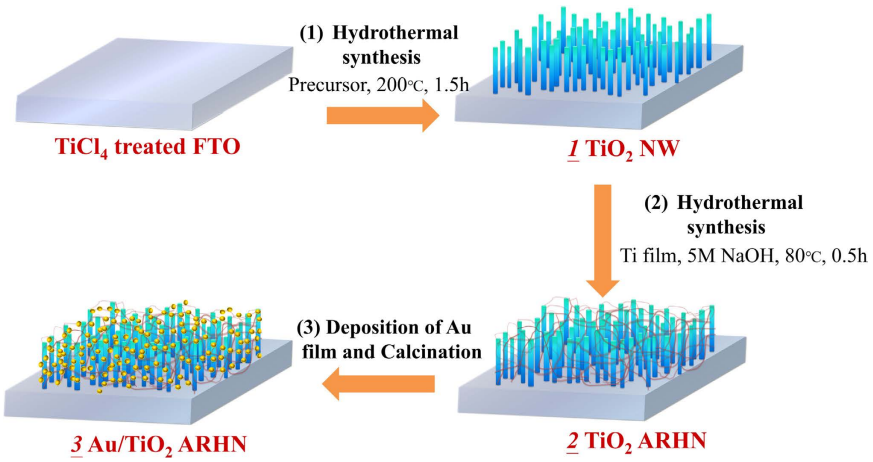

Figure 2. Schematic description of the synthesis process of TiO_2 NWs, ARHN and Au/TiO_2 ARHN on FTO substrates.

electromagnetic coupling of the Au NPs, the solid support——TiO_2 NWs connected with TiO_2 threads—— was synthesized by a two-step hydrothermal process. When tested in the PEC experiment, the TiO_2 ARHN and Au/TiO_2 ARHN exhibited 1.5 times and 4.5 times higher photocurrent than TiO_2 NWs.

Results and Discussion

Figure 2 schematically depicts the three-step fabrication process of reproducible Au/TiO_2 ARHN. Figure 3a represents a top-view SEM image of the TiO_2 NWs. The light-gray needle-like regions in the SEM image represent the TiO_2 NWs and the dark regions are the underlying FTO substrate. A cross-sectional SEM image of the NWs (Fig. 3b) shows that the thickness of TiO_2 layer is ~1 μm and the NWs have an average diameter of 40 nm. XRD patterns of the TiO_2 NWs show predominantly rutile phase with preferential orientation of (110) (Supplementary Fig. 1). The top-view and cross-sectional SEM image of the TiO_2 ARHN (Fig. 3c,d) shows that the TiO_2 threads are bridged with the TiO_2 NWs to form a 3D hierarchical network. Nest-like porous cavities with diameters of a few hundred nanometers are clearly observed and the diameters of the threads are ~10 nm. The XRD patterns and Raman spectra show that the threads belong to the anatase phase (Supplementary Figs 2 and 3). The top-view SEM image of the Au/TiO_2 ARHN is shown in Fig. 3e. The white dot regions in the SEM represent the Au NPs. The size distribution histograms of Au NPs show an average particle size of 15 nm (Fig. 3f).

To investigate the formation mechanism of TiO_2 ARHN, a series of experiments were performed. Firstly, we failed to obtain TiO_2 ARHN without $TiCl_4$ treatment. We found that TiO_2 threads cannot grow on TiO_2 NWs with a smooth surface. Secondly, in the absence of the Ti film in step 2 (in Fig. 2), only TiO_2 NWs were observed. These findings suggest that both $TiCl_4$ treatment and the formation of the Ti layer for the formation of TiO_2 ARHN are indispensable. Therefore, we propose that small TiO_2 seed crystals grow on the surface of TiO_2 NWs after $TiCl_4$ treatment, which leads to a rough surface for the growth of TiO_2 threads. Moreover, during alkali

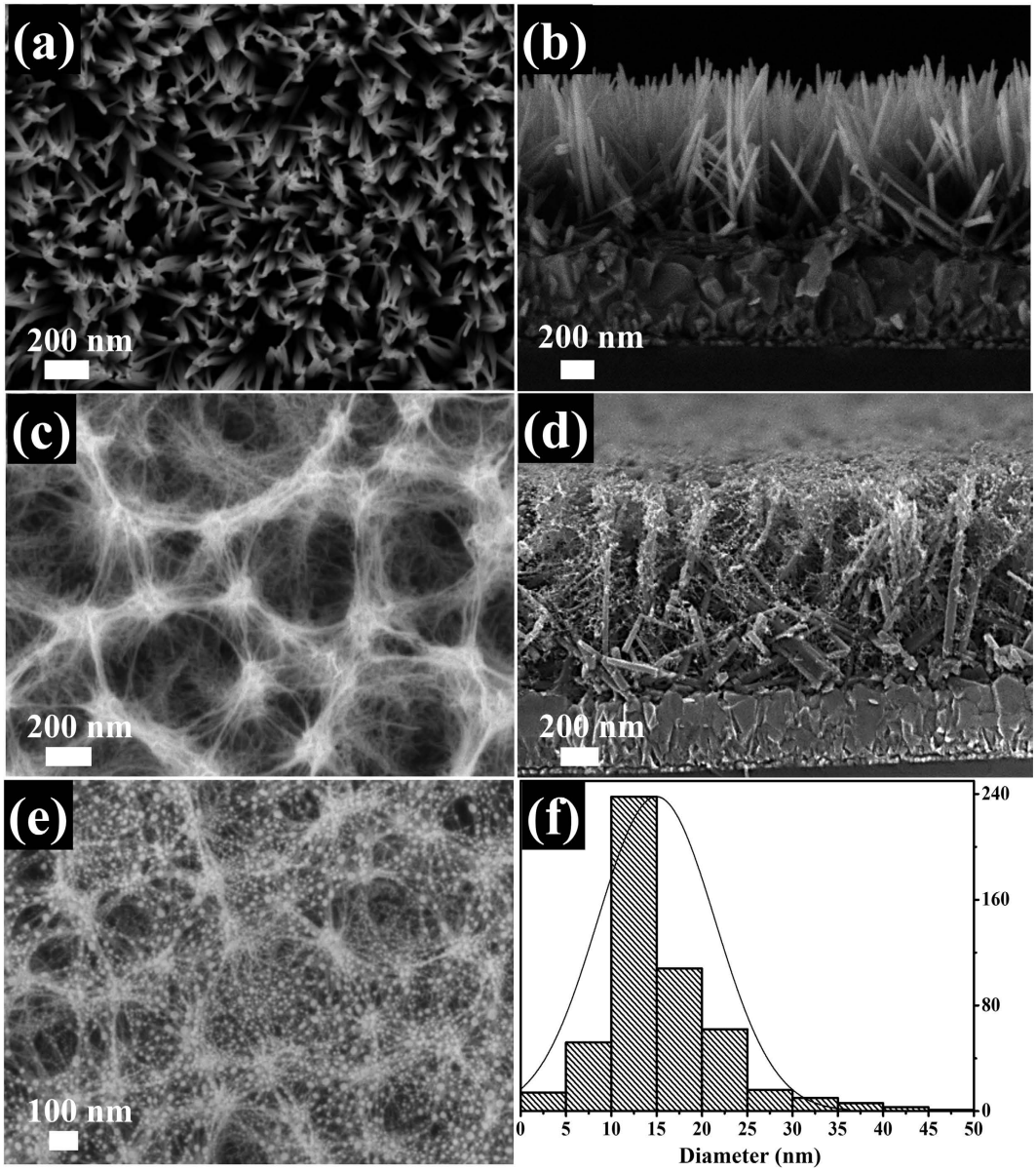

Figure 3. FESEM images. (**a**,**c**,**e**) top images of top TiO_2 NW, TiO_2 ARHN and Au/TiO_2 ARHN, respectively; (**b**,**d**) cross-sectional images of TiO_2 NW and TiO_2 ARHN; (**f**) the size distribution of Au NPs.

hydrothermal process, the Ti layers can generate large amounts of Ti-containing species[37,38] as precursors that can deposit on the TiO_2 seeds and produce a network structure.

To evaluate the enhanced PEC performance of the designed Au/TiO_2 ARHN, the linear sweep voltammograms and the photocurrent-versus-time (I-t curve) of TiO_2 NW and TiO_2 ARHN with/without Au NPs were conducted under AM 1.5 G simulated solar illumination, as shown in Fig. 4. The measured photocurrent was normalized to the sample area to obtain the photocurrent density for comparison. As presented in Fig. 4a, the TiO_2 NW electrode produced a photocurrent density of 4×10^{-5} A cm^{-2} at 0.23 V *vs*. Ag/AgCl, which is the potential often chosen as a metric to evaluate the performance of photoanodes as it corresponds to the water oxidation potential[4]. The low photocurrent density is attributed to the limit of wide band-gap characteristics of TiO_2 (3.2 eV for anatase[39] and 3.0 eV for rutile[40]), due to which only UV light can be used in the PEC water splitting system. The photocurrent was enhanced for the TiO_2 ARHN (6×10^{-5} A cm^{-2}) when compared with TiO_2 NW, with an enhancement factor of 1.5. As expected, a significant photocurrent density enhancement was clearly observed on the Au/TiO_2 ARHN, having a photocurrent density of 1.8×10^{-4} A cm^{-2}. As compared to TiO_2 NW, a photocurrent enhancement higher than 4.5 times was achieved. From Fig. 4b, all electrode represent a good reproducibility and stability as the illumination was turned on and off. Furthermore, the sharp spike in the photocurrent during the on/off illumination cycles demonstrates the predominant transport of photogenerated electrons in the designed TiO_2 structure[41].

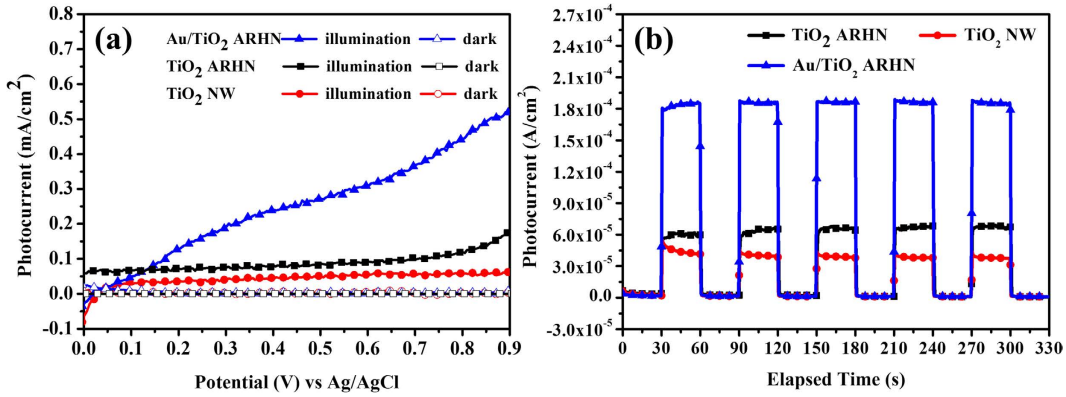

Figure 4. (**a**) Linear sweep voltammograms and (**b**) amperometric I——t curves of TiO_2 NW, TiO_2 ARHN and Au/TiO_2 ARHN photoelectrode.

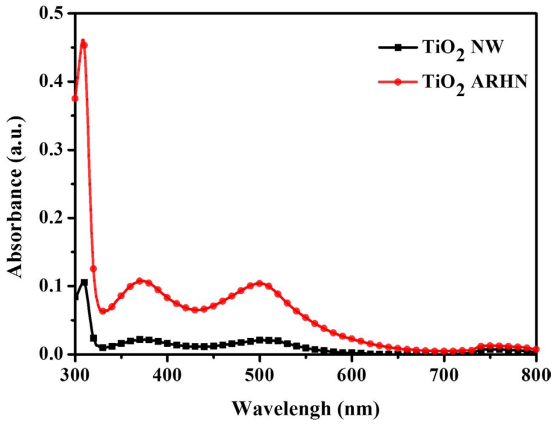

Figure 5. UV-Vis spectra of desorbed N719 solution.

We suggest the enhanced photocurrent of TiO_2 ARHN electrode could be attributed to better photocatalytic activity, due to increased surface area, or better light harvest efficiency, due to the hierarchical network structure. Therefore, the dye absorption/desorption experiment and UV-visible spectrum measurement were perform to verify it. Here, dye N719 was choose as an adsorbate to execute dye absorption/desorption experiment due to it could be monolayer absorbed on the surface of TiO_2. Therefore, we can evaluate the related surface area via measuring the absorption of N719 dye which detach from TiO_2 structure. As shown in Fig. 5, there are three absorbed peak of N719 located on 310 nm, 370 nm and 505 nm, respectively[42]. It is observed that the absorption of detached N719 solution based on TiO_2 ARHN is obviously large than TiO_2 NW on entire spectrum. It represents the surface area of TiO_2 ARHN is related large than TiO_2 NW due to there are more dye absorbed on TiO_2 ARHN. Based on the result, we make a sure that the high surface area of TiO_2 ARHN is a reasonable reason which bring to a high photo activity on PEC measurement.

Furthermore, the UV-visible absorption spectra of the TiO_2 NW and TiO_2 ARHN with/without Au NPs are shown in Fig. 6. TiO_2 NW exhibits a stronger absorption at the wavelengths below 400 nm due to electron transitions of TiO_2 from the valence band to the conduction band. In addition, the absorption spectra of TiO_2 ARHN showed an enhanced absorption in the entire spectral range as compared with TiO_2 NW, which is attributed to the scattering effect in the ARHN structure; this also explains the increased photocurrent in the TiO_2 ARHN. With deposited Au NPs, the absorption show a significantly enhancement on visible range which is driven by the LSPR absorption. From incident photon-to-electron conversion efficiency (IPCE) measurement (Supplementary Fig. 4), it demonstrates that such an absorption successfully boosts the PEC performance in the region from 400 nm to 700 nm.

In this work, a LSPR peak for the Au NPs with average size of 15 nm centered at around 540 nm. For Au NPs of size 10–20 nm, the absorption peak of plasmon resonance is usually located at 520–525 nm[43,44]. A redshift of 15–20 nm of the plasmon resonance peak was observed as compared to previous reports. This may be attributed to the TiO_2 changing the surrounding dielectric property of Au NPs (Au NPs well deposited and in contact withTiO_2 surface) and the enhancement of electromagnetic field of LSPR[30,45,46]. It has been reported that the high electromagnetic field of LSPR and strong coupling between Au NPs and TiO_2 will benefit the plasmon-induced charge transportation and separation, enabling SPR-enhanced photocatalysis. Typically, the LSPR-induced charge separation at the interface between the Au NPs and TiO_2 can occur by transferring the energy contained in the oscillating electrons or local plasmonic field from Au NPs to TiO_2 through direct electron transfer, also known

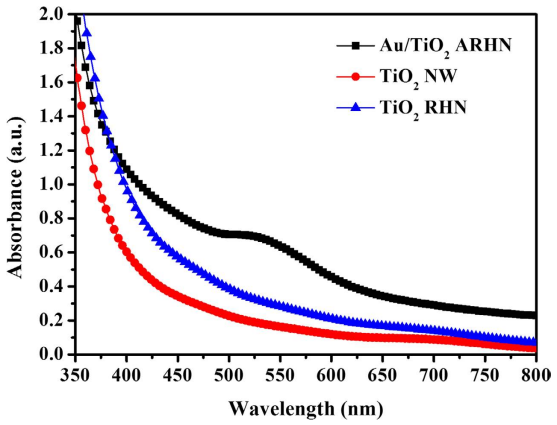

Figure 6. UV-Vis spectra of TiO_2 NW, TiO_2 ARHN and Au/TiO_2 ARHN.

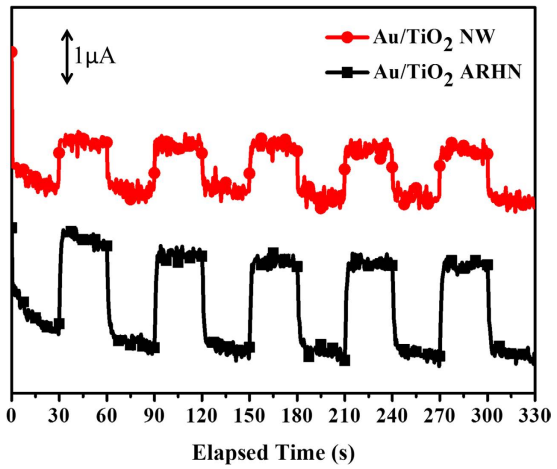

Figure 7. I — t curves collected at 0 V versus Ag/AgCl for Au/TiO_2 NW and Au/TiO_2 ARHN electrode under visible light illumination (using a cutoff filter with a wavelength of 400 nm).

as hot electron injection[47,48]. Higher electromagnetic field generates more hot electron[49,50]. In order to verify our assumption, the design of TiO_2 ARHN is helpful to improve electromagnetic field as compared to NWs, the PEC measurement was performed to check the hot electron effect. Figure 7 shows the I-t curve measured under visible-light illumination. From Fig. 7, it is obvious that the photocurrent of Au/TiO_2 ARHN is two times higher than Au/TiO_2 NW. It means that the high plasmon electromagnetic field of Au/TiO_2 ARHN results in a high hot-electron current. Therefore, we confirm that the design of TiO_2 ARHN successfully provides a model for strengthening LSPR ability and demonstrates a remarkable enhancement on PEC performance.

In this study, we are further interested the effectiveness of density effect and size effect on the performance of photo electrochemical property. The related data and discussion were shown in Supplementary Information. In addition, the stability test and Faradaic efficiency were obtained. Under continuously illumination for 10800 seconds (equal to 3 hr), the photocurrent density was decrease from 1.8×10^{-4} A/cm^2 to 1.5×10^{-4} A/cm^2 in the case of Au/TiO_2 ARHN, as shown in Fig. 8a. This photocurrent decay is similar to previous report[51]. We suggest it could be attributed to photo induced corrosion which competes with water oxidation reaction[51]. However, such a corrosion could be suppress by surface treatment of TiO_2 nanostructure or use of sacrificial reagent/catalyst for longstanding application[51]. From Fig. 8b, the calculated Faradaic efficiency exceed 90% and 85% for TiO_2 ARHN and Au/TiO_2 ARHN, respectively. The high value of Faradaic efficiency of oxygen gas during 10 hr demonstrated that the photo generated current indeed utilized for water oxidation. Also, we could observe hydrogen gas from real picture as shown inset diagram in Fig. 8c. Therefore, we propose the electron transfer mechanism in Au/TiO_2 ARHN system as shown in Fig. 8c. Under illumination, Au NPs absorb visible light, generating the energetic hot electrons from the process of SP excitation, and injecting them into the conduction band of the adjacent TiO_2 (green arrow). Simultaneously, the UV light is absorbed by TiO_2, producing a photo-excited electron and a hole (black arrow). The plasmon-induced electromagnetic field promotes the separation of photogenerated electrons and holes. Furthermore, as illustrated, the energy bands of anatase and rutile are different which provides a driving force to promote electron transfer from anatase to rutile (blue arrow). Finally, the electrons transferred to the cathode (Pt) react with H^+ ions and produce H_2 (pink arrow) whereas the holes present in the anode oxidize H_2O and generate O_2.

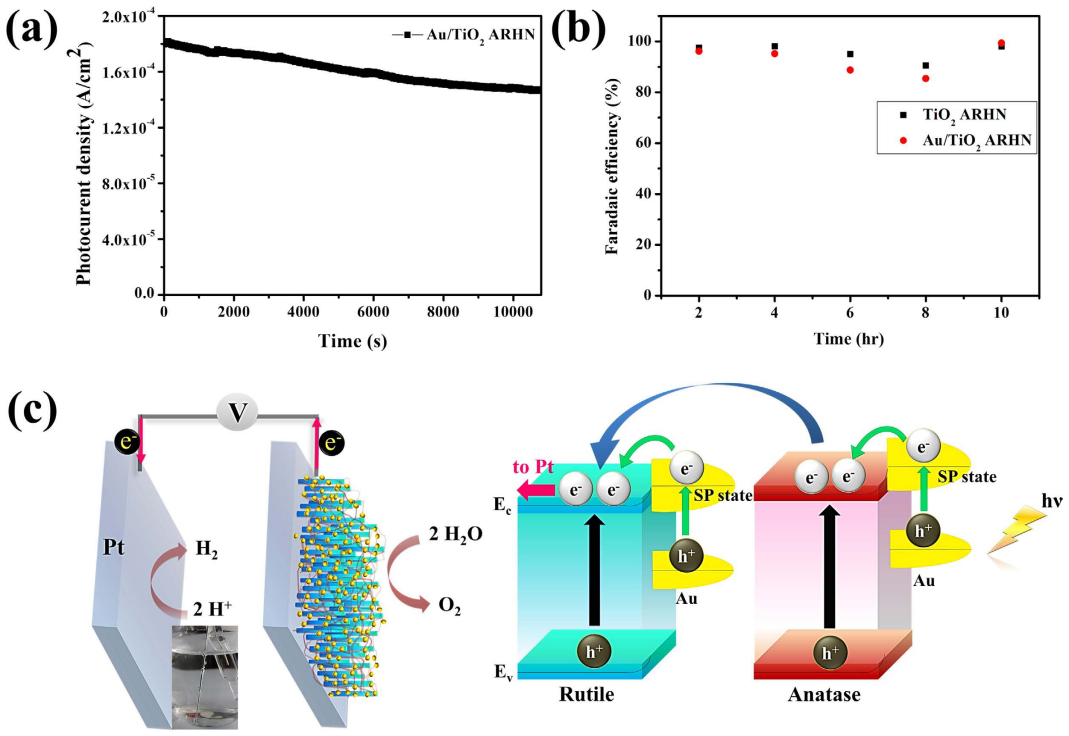

Figure 8. (**a**) Current——time curves of Au/TiO_2 ARHN collected in 1 M NaOH at 0.23 V vs Ag/AgCl under 100 mW/cm^2 for 3 h. (**b**) The calculated Faradaic efficiency for O_2 gas evolution. (**c**) Charge transfer mechanism of Au/TiO_2 ARHN under solar illumination.

In conclusion, this work demonstrates a plasmon-induced effect on a designed 3D web architecture constructed from rutile TiO_2 NWs, anatase TiO_2 threads and Au NPs. Such a nanostructure was achieved for the first time through a simple and inexpensive hydrothermal procedure followed by calcination. The PEC performance tests, reveal that the photocurrent of Au/TiO_2 ARHN was 4.5 times greater than that of the TiO_2 NW photoelectrode. The observed optical properties and dark current measurements confirm that the excellent PEC performance of Au/TiO_2 ARHN was due to three reasons: (1) the high surface area of TiO_2 ARHN that increase the photoactive center, (2) the scattering effect in the TiO_2 ARHN and the LSPR properties of Au NPs that enhanced the light harvest, (3) the strength coupling effect between Au NPs and TiO_2 nanostructure that accelerated the charge transportation and separation. The mechanism of charge transportation in the Au/TiO_2 ARHN was proposed based on our findings. Practical use of the Au/TiO_2 ARHN was demonstrated to indicate their significant potential for use in photoelectric conversion system.

Methods

Materials. F:SnO_2 (FTO) (1.5 cm × 3 cm, TEC-7, 7 ohm/sq., 2.2 mm thick) was used as the substrate for growth of the TiO_2 film. All chemicals were used without further purification. Sodium hydroxide (NaOH, 99%), titanium tetrachloride ($TiCl_4$, 99%), 2-butanone (C_4H_8O, >99%), hydrochloric acid (HCl, 12 M) and nitric acid (HNO_3, 65%) were purchased from Merck. Tetrabutyl titanate ($C_{16}H_{36}O_4Ti$, >97%) and ruthenium 535 bis-TBA (N719 dye) were obtained from Aldrich and Solaronix, respectively.

Hydrothermal synthesis of TiO_2 NWs on FTO substrates. First, FTO was cleaned by ultrasonic agitation in a mixture of ethanol, acetone and deionized water (volume ratio of 1:1:1) for 15 min. The FTO substrates were immersed in an aqueous of 0.5 M $TiCl_4$ at 80 °C for 30 min, followed by heat treatment at 500 °C for 30 min to yield a thin TiO_2 layer. The $TiCl_4$-treated substrates were then suspended in a reagent solution containing 6 mL HCl, 6 mL 2-butanone and 0.6 mL tetrabutyl titanate in a Teflon vessel. The Teflon vessel was sealed in an autoclave and heated at 200 °C for 1.5 h. Further annealing at 500 °C for 30 min resulted in the growth of crystalline TiO_2 NWs on FTO substrates[52].

Hydrothermal synthesis of TiO_2 ARHN on FTO substrates. The TiO_2 NW substrate (without calcination) was first treated with $TiCl_4$ solution as mentioned above. A 200-nm-thick Ti layer was sputtered on the $TiCl_4$-treated TiO_2 NW using a magnetic sputter (K575X, Quorum Technologies). The substrates were then transferred to a Teflon vessel with the addition of a 5 M aqueous NaOH solution and were encapsulated in a stainless-steel autoclave. Then, the autoclave was heated at 80 °C for 30 min. After the low-temperature hydrothermal process, the substrate was rinsed with 0.1 M HNO_3 followed by deionized water, and was finally calcined at 500 °C for 30 min to obtain hierarchical nanostructures.

Synthesis of Au/TiO_2 ARHN. A 5-nm Au layer was sputtered on the TiO_2 NW and ARHN using a magnetic sputter. The Au deposited TiO_2 were subsequently calcined at 500 °C for 1 h to obtain Au/TiO_2 ARHN.

Characterizations and measurements. The surface and cross-section morphologies of samples were examined by field-emission scanning electron microscopy (FE-SEM, Zeiss Ultraplus). The SigmaScan Pro 5 software was used to calculate particle size (300 particles were counted). The crystal structure was characterized by X-ray diffraction (XRD, PANalytical X'Pert Pro MRD) and Raman spectroscopy (Tokyo Instruments, INC). A UV/Vis spectrometer (Perkin Elmer/Lambda 900) was used to obtain the absorption spectra. The dye absorption/desorption experiment was performed by desorbing a dye-sensitized TiO_2 electrode in a 0.1 M NaOH solution in 1:1 H_2O/EtOH[53]. Subsequently, a UV–vis spectrometer was introduced to measure the absorbance of the desorbing solution. The electrochemical measurement was carried out using three-electrode system. TiO_2 electrode with or without Au NPs was the working electrode; an Ag/AgCl (3 M KCl) electrode in saturated KCl was the reference electrode; the Pt plate was used as the counter electrode. All PEC cells were examined in 1 M NaOH solution with a PARSTAT 2263 Advanced Electrochemical System under illumination by Newport solar simulator with AM 1.5 G (100 mW/cm^2). The incident photon-to-current conversion efficiency (IPCE) was measured with an action spectrum measurement setup (Peccell, PEC-S20).

References

1. Fujishima, A. & Honda, K. Electrochemical Photolysis of Water at a Semiconductor Electrode. *Nature* **238,** 37–38 (1972).
2. Zhao, Y. *et al.* Uniform Mesoporous Anatase Hollow Spheres: An Unexpectedly Efficient Fabrication Process and Enhanced Performance in Photocatalytic Hydrogen Evolution. *Chemistry-A European Journal* (2014).
3. Yang, X. H. *et al.* Ultra-Thin Anatase TiO_2 Nanosheets Dominated with {001} Facets: Thickness-Controlled Synthesis, Growth Mechanism and Water-Splitting Properties. *CrystEngComm* **13,** 1378–1383 (2011).
4. Zhang, Z. & Wang, P. Optimization of Photoelectrochemical Water Splitting Performance on Hierarchical TiO_2 Nanotube Arrays. *Energy & Environmental Science* **5,** 6506–6512 (2012).
5. Chen, B., Hou, J. & Lu, K. Formation Mechanism of TiO_2 Nanotubes and Their Applications in Photoelectrochemical Water Splitting and Supercapacitors. *Langmuir* **29,** 5911–5919 (2013).
6. Wang, D. *et al.* Photoelectrochemical Water Splitting with Rutile TiO_2 Nanowires Array: Synergistic Effect of Hydrogen Treatment and Surface Modification with Anatase Nanoparticles. *Electrochimica Acta* **130,** 290–295 (2014).
7. Huang, W., Wang, X., Xue, Y., Yang, Y. & Ao, X. Hybrid Nanostructures of Mixed-Phase TiO_2 for Pnhanced Photoelectrochemical Water Splitting. *RSC Advances* **5,** 56098–56102 (2015).
8. Wolcott, A., Smith, W. A., Kuykendall, T. R., Zhao, Y. & Zhang, J. Z. Photoelectrochemical Water Splitting Using Dense and Aligned TiO_2 Nanorod Arrays. *Small* **5,** 104–111 (2009).
9. Bard, A. J. & Fox, M. A. Artificial Photosynthesis: Solar Splitting of Water to Hydrogen and Oxygen. *Accounts of Chemical Research* **28,** 141–145 (1995).
10. Lou, Y. & Chen, J. Recent Developments in One Dimensional (1D) Nanostructured TiO_2 for Photoelectrochemical Water Splitting. *Nanoscience and Nanotechnology Letters* **6,** 361–371 (2014).
11. Cho, I. S. *et al.* Branched TiO_2 Nanorods for Photoelectrochemical Hydrogen Production. *Nano Letters* **11,** 4978–4984 (2011).
12. Lee, D. *et al.* Synthesis of Hierarchical TiO_2 Nanowires with Densely-Packed and Omnidirectional Branches. *Nanoscale* **5,** 11147–11152 (2013).
13. Bai, H., Liu, L., Liu, Z. & Sun, D. D. Hierarchical 3D Dendritic TiO_2 Nanospheres Building with Ultralong 1D Nanoribbon/Wires for High Performance Concurrent Photocatalytic Membrane Water Purification. *Water Research* **47,** 4126–4138 (2013).
14. Chang, M.-L. & Li, X.-J. Fabrication of Nanosheet/Nestlike Nanoarray Hierarchical TiO_2 Film for Dye-Sensitized Solar Cell. *Acta Physico-Chimica Sinica* **28,** 1368–1372 (2012).
15. Wang, H. *et al.* Rutile TiO_2 Nano-Branched Arrays on FTO for Dye-Sensitized Solar Cells. *Physical Chemistry Chemical Physics* **13,** 7008–7013 (2011).
16. Liao, W.-P. & Wu, J.-J. Wet Chemical Route to Hierarchical TiO_2 Nanodendrite/Nanoparticle Composite Anodes for Dye-Sensitized Solar Cells. *Journal of Materials Chemistry* **21,** 9255–9262 (2011).
17. Hu, A., Li, H., Jia, Z. & Xia, Z. TiO_2 Nanorods Branched on Fast-Synthesized Large Clearance TiO_2 Nanotube Arrays for Dye-Sensitized Solar Cells. *Journal of Solid State Chemistry* **184,** 2936–2940 (2011).
18. Zhuge, F. *et al.* Toward Hierarchical TiO_2 Nanotube Arrays for Efficient Dye-Sensitized Solar Cells. *Advanced Materials* **23,** 1330–1334 (2011).
19. Hu, A. *et al.* Two Novel Hierarchical Homogeneous Nanoarchitectures of TiO_2 Nanorods Branched and P25-Coated TiO_2 Nanotube Arrays and Their Photocurrent Performances. *Nanoscale. Res. Lett* **6,** 2–6 (2011).
20. Liao, J.-Y., Lei, B.-X., Chen, H.-Y., Kuang, D.-B. & Su, C.-Y. Oriented Hierarchical Single Crystalline Anatase TiO_2 Nanowire Arrays on Ti-Foil Substrate for Efficient Flexible Dye-Sensitized Solar Cells. *Energy & Environmental Science* **5,** 5750–5757 (2012).
21. Liu, Z.-H. *et al.* Hierarchical TiO_2 Nanorod Array for Dye-Sensitized Solar Cells. *Materials Letters* **89,** 309–311 (2012).
22. Wu, W.-Q. *et al.* Dye-Sensitized Solar Cells Based on a Double Layered TiO_2 Photoanode Consisting of Hierarchical Nanowire Arrays and Nanoparticles with Greatly Improved Photovoltaic Performance. *Journal of Materials Chemistry* **22,** 18057–18062 (2012).
23. Yang, J.-S., Liao, W.-P. & Wu, J.-J. Morphology and Interfacial Energetics Controls for Hierarchical Anatase/Rutile TiO_2 Nanostructured Array for Efficient Photoelectrochemical Water Splitting. *ACS Applied Materials & Interfaces* **5,** 7425–7431 (2013).
24. Tian, H., Zhao, G., Zhang, Y.-n., Wang, Y. & Cao, T. Hierarchical (0 0 1) Facet Anatase/Rutile TiO_2 Heterojunction Photoanode with Enhanced Photoelectrocatalytic Performance. *Electrochimica Acta* **96,** 199–205 (2013).
25. Kim, D. H. *et al.* Anatase TiO_2 Nanorod-Decoration for Highly Efficient Photoenergy Conversion. *Nanoscale* **5,** 11725–11732 (2013).
26. Rayalu, S. S. *et al.* Photocatalytic Water Splitting on Au/TiO_2 Nanocomposites Synthesized Through Various Routes: Enhancement in Photocatalytic Activity Due to SPR Effect. *Applied Catalysis B: Environmental* **142–143,** 684–693 (2013).
27. DeSario, P. A. *et al.* Plasmonic Enhancement of Visible-Light Water Splitting with Au-TiO_2 Composite Aerogels. *Nanoscale* **5,** 8073–8083 (2013).
28. Reichert, R., Jusys, Z. & Behm, R. J. Au/TiO_2 Photo (electro) catalysis: The Role of the Au Cocatalyst in Photoelectrochemical Water Splitting and Photocatalytic H_2 Evolution. *The Journal of Physical Chemistry C* **119,** 24750–24759 (2015).
29. Pu, Y.-C. *et al.* Au Nanostructure-Decorated TiO_2 Nanowires Exhibiting Photoactivity Across Entire UV-Visible Region for Photoelectrochemical Water Splitting. *Nano Letters* **13,** 3817–3823 (2013).
30. Seh, Z. W. *et al.* Janus Au-TiO_2 Photocatalysts with Strong Localization of Plasmonic Near-Fields for Efficient Visible-Light Hydrogen Generation. *Advanced Materials* **24,** 2310–2314 (2012).
31. Zhang, Z., Zhang, L., Hedhili, M. N., Zhang, H. & Wang, P. Plasmonic Gold Nanocrystals Coupled with Photonic Crystal Seamlessly on TiO_2 Nanotube Photoelectrodes for Efficient Visible Light Photoelectrochemical Water Splitting. *Nano Letters* **13,** 14–20 (2013).

32. Mukherjee, S. *et al.* Hot Electrons Do the Impossible: Plasmon-Induced Dissociation of H_2 on Au. *Nano Letters* **13,** 240–247 (2013).
33. Qian, K. *et al.* Surface Plasmon-Driven Water Reduction: Gold Nanoparticle Size Matters. *Journal of the American Chemical Society* **136,** 9842–9845 (2014).
34. Zhan, Z., An, J., Zhang, H., Hansen, R. V. & Zheng, L. Three-Dimensional Plasmonic Photoanodes Based on Au-Embedded TiO_2 Structures for Enhanced Visible-Light Water Splitting. *ACS Applied Materials & Interfaces* **6,** 1139–1144 (2014).
35. Kim, H. J. *et al.* Plasmon-Enhanced Photoelectrochemical Water Splitting with Size-Controllable Gold Nanodot Arrays. *ACS Nano* **8,** 10756–10765 (2014).
36. Wang, H., You, T., Shi, W., Li, J. & Guo, L. Au/TiO_2/Au as a Plasmonic Coupling Photocatalyst. *The Journal of Physical Chemistry C* **116,** 6490–6494 (2012).
37. Wu, D. *et al.* Sequence of Events for the Formation of Titanate Nanotubes, Nanofibers, Nanowires, and Nanobelts. *Chemistry of Materials* **18,** 547–553 (2006).
38. Yen, Y.-C., Chen, P.-H., Chen, J.-Z., Chen, J.-A. & Lin, K.-J. Plasmon-Induced Efficiency Enhancement on Dye-Sensitized Solar Cell by a 3D TNW-AuNP Layer. *ACS Applied Materials & Interfaces* **7,** 1892–1898 (2015).
39. Linsebigler, A. L., Lu, G. & Yates, J. T. Photocatalysis on TiO_2 Surfaces: Principles, Mechanisms, and Selected Results. *Chemical Reviews* **95,** 735–758 (1995).
40. Pascual, J., Camassel, J. & Mathieu, H. Fine Structure in the Intrinsic Absorption Edge of TiO_2. *Physical Review B* **18,** 5606–5614 (1978).
41. Kim, K., Thiyagarajan, P., Ahn, H.-J., Kim, S.-I. & Jang, J.-H. Optimization for visible light photocatalytic water splitting: gold-coated and surface-textured TiO_2 inverse opal nano-networks. *Nanoscale* **5,** 6254–6260, doi: 10.1039/C3NR01552A (2013).
42. Han, H.-G. *et al.* Ultrafast Fabrication of Flexible Dye-Sensitized Solar Cells by Ultrasonic Spray-Coating Technology. *Scientific Reports* **5,** 14645 (2015).
43. Link, S. & El-Sayed, M. A. Spectral Properties and Relaxation Dynamics of Surface Plasmon Electronic Oscillations in Gold and Silver Nanodots and Nanorods. *The Journal of Physical Chemistry B* **103,** 8410–8426 (1999).
44. Jelveh, S. & Chithrani, D. B. Gold Nanostructures as a Platform for Combinational Therapy in Future Cancer Therapeutics. *Cancers* **3,** 1081 (2011).
45. Chen, C.-F., Tzeng, S.-D., Chen, H.-Y., Lin, K.-J. & Gwo, S. Tunable Plasmonic Response from Alkanethiolate-Stabilized Gold Nanoparticle Superlattices: Evidence of Near-Field Coupling. *Journal of the American Chemical Society* **130,** 824–826 (2008).
46. Kawawaki, T., Takahashi, Y. & Tatsuma, T. Enhancement of Dye-Sensitized Photocurrents by Gold Nanoparticles: Effects of Plasmon Coupling. *The Journal of Physical Chemistry C* **117,** 5901–5907 (2013).
47. Li, J. *et al.* Plasmon-Induced Photonic and Energy-Transfer Enhancement of Solar Water Splitting by a Hematite Nanorod Array. *Nat Commun* **4** (2013).
48. Cushing, S. K. *et al.* Controlling Plasmon-Induced Resonance Energy Transfer and Hot Electron Injection Processes in Metal@TiO_2 Core–Shell Nanoparticles. *The Journal of Physical Chemistry C* **119,** 16239–16244 (2015).
49. Kazuma, E., Sakai, N. & Tatsuma, T. Nanoimaging of Localized Plasmon-Induced Charge Separation. *Chemical Communications* **47,** 5777–5779 (2011).
50. Yang, T.-H. *et al.* Ultrahigh Density Plasmonic Hot Spots with Ultrahigh Electromagnetic Field for Improved Photocatalytic Activities. *Applied Catalysis B: Environmental* **181,** 612–624 (2016).
51. Yang, Y. *et al.* Photohole Induced Corrosion of Titanium Dioxide: Mechanism and Solutions. *Nano letters* **15,** 7051–7057 (2015).
52. Feng, X., Zhu, K., Frank, A. J., Grimes, C. A. & Mallouk, T. E. Rapid Charge Transport in Dye-Sensitized Solar Cells Made from Vertically Aligned Single-Crystal Rutile TiO_2 Nanowires. *Angewandte Chemie International Edition* **51,** 2727–2730, doi: 10.1002/anie.201108076 (2012).
53. Dell'Orto, E., Raimondo, L., Sassella, A. & Abbotto, A. Dye-sensitized solar cells: spectroscopic evaluation of dye loading on TiO_2. *Journal of Materials Chemistry* **22,** 11364–11369 (2012).

Acknowledgements

We greatly acknowledge financial support from the Ministry of Science and Technology of Taiwan (104-2113-M-005 -011 -MY3; 105-2811-M-005-020). We would like to thank Prof. Hao-Ming Chen from National Taiwan University for his cooperation in the measurement and calculation of Faradaic efficiency and Prof. Chen-Yu Yeh from National Chung Hsing University for his kindly help in the IPCE measurement.

Author Contributions

Y.C.Y. and K.J.L. conceived and design the project. J.A.C., S.O. and Y.S.C. conducted experimental work. Y.C.Y. and J.A.C. analyzed the data. Y.C.Y. wrote the main manuscript text. All authors discussed the results and reviewed the manuscript.

Additional Information

Supplementary information accompanies this paper at http://www.nature.com/srep

Competing financial interests: The authors declare no competing financial interests.

How to cite this article: Yen, Y.-C. *et al.* Plasmon-Enhanced Photocurrent using Gold Nanoparticles on a Three-Dimensional TiO_2 Nanowire-Web Electrode. *Sci. Rep.* **7**, 42524; doi: 10.1038/srep42524 (2017).

Publisher's note: Springer Nature remains neutral with regard to jurisdictional claims in published maps and institutional affiliations.